Journal of Materials Chemistry A

Modification of $LiNi_{0.5}Mn_{1.5}O_4$ high potential cathode from the inner lattice to the outer surface with Cr^{3+}-doping and Li^+-conductor coating

Journal:	*Journal of Materials Chemistry A*
Manuscript ID:	TA-COM-02-2014-000974.R2
Article Type:	Communication
Date Submitted by the Author:	09-May-2014
Complete List of Authors:	Yang, Xiaojian; Changzhou university, Yang, Tao; Changzhou university, Liang, Shanshan; Changzhou university, Wu, Xin; Changzhou university, Zhang, Hanping; Changzhou university,

Modification of $LiNi_{0.5}Mn_{1.5}O_4$ high potential cathode from the inner lattice to the outer surface with Cr^{3+}-doping and Li^+-conductor coating

Xiaojian Yang, Tao Yang, Shanshan Liang, Xin Wu and Hanping Zhang*

Received (in XXX, XXX) Xth XXXXXXXXX 20XX, Accepted Xth XXXXXXXXX 20XX

DOI: 10.1039/b000000x

An approach to simultaneously modifying spinel $LiNi_{0.5}Mn_{1.5}O_4$ cathode from the interior to the exterior is demonstrated. The Cr^{3+}-doping effectively eliminates the $Li_xNi_{1-x}O$ impurity phase and improves the structural stability. The introduced $Li_{0.1}B_{0.967}PO_4$ coating layer which acts as an ion-conductor provides both a favourable Li^+ diffusion channel at intergranular interface and a stable protection shell on the surface of particles. Owing to the combined effect of Cr^{3+}-doping and Li^+-conductor coating, $LiNi_{0.5}Mn_{1.5}O_4$ material exhibits excellent cycle stability and rate performance at high output voltage.

Lithium ion batteries are great commercial successes in portable electric devices owing to their high energy densities and long cycle lives. In today's energy-based society[1], lithium ion batteries are trying to expand to some important fields such as renewable energy storage and electric vehicles (EVs). However, two concerns have to be circumvented before a large-scale application in these fields comes into being. In one side, the current batteries can basically store the renewable solar and wind energies, but they are still very expensive. In another side, they can drive the electric car, but their energy and power are not high enough.[2,3] Cathode materials are one of the key issues to solve these problems. And the $LiNi_{0.5}Mn_{1.5}O_4$ (LNMO) compounds are appealing cathode candidates for lithium ion batteries which are mainly studied for high energy applications like automotive industry due to their high energy density (650 Wh kg^{-1}) at a high operating voltage up to 4.7 V.[4–6]

However, LNMO shows serious capacity fade due to the generation of $Li_xNi_{1-x}O$ impurity phase in the synthesis process[7] and the large lattice strain during cycling, which involves the formation of three cubic phases with a large lattice parameter difference during the charge-discharge process.[8,9] Furthermore, the corrosion reactions between the high-voltage charged cathode and the electrolyte[10–13] result in high interfacial cell impedance and poor cell electrochemical performance.[14]

Accordingly, the methods of lattice doping and surface coating have been put forward. It has been found that the cationic substitutions can eliminate the formation of the $Li_xNi_{1-x}O$ impurity phase and stabilize the spinel structure with a disordering of the Mn^{4+} and Ni^{2+} ions in the 16d octahedral sites, leading to prolonged cycle life.[7] Among various ionic dopings, Cr^{3+}-doping is impressing. Recent work has demonstrated that the substitution of a small amount of Cr eliminated the impurity phase without changing the $Fd\bar{3}m$ space group, bringing benefit to the $LiNi_{0.5}Mn_{1.5}O_4$ performance.[15] On the other hand, the coating approach contributes to suppress the side reactions between the electrode surface and the electrolytes. As has been reported, $LiNi_{0.42}Co_{0.16}Mn_{1.42}O_4$ coated with nanosized Al_2O_3, ZnO and

Bi_2O_3 manifested better cyclability than bare sample.[7]

Recently, functional coating using Li^+-conductor as the cover layer had been carried out.[16–18] The coating layer can facilitate the Li^+ passing through and of course, can protect the substrate against the attack from the electrolyte. For LNMO cathode material, the integrated functional materials which possess both cationic doped inner and Li^+-conductor coated surface may provide us a great chance to obtain high performance batteries.

$Li_{0.1}B_{0.967}PO_4$ (LBPO) has been investigated as solid electrolyte for all-solid lithium ion batteries owing to the high lithium ionic conductivity (in the order of 10^{-4} S cm^{-1}).[19] Here we introduce the material as an active-coating layer to modify the ionic conductivity of the Cr^{3+} doped host, $LiNi_{0.45}Cr_{0.1}Mn_{1.45}O_4$ (Cr-LNMO). As a result, a good compatibility between LBPO coating and Cr^{3+}-doping is achieved. The result indicates a successful example to obtain an integrating modification from the interior lattice to the exterior surface for high potential cathode materials.

The typical synthesis procedure is illustrated in Scheme 1. Cr-LNMO particles were firstly synthesized by adopting a soft combustion reaction between CH_3COOLi, $Mn(CH_3COO)_2$, $Ni(NO_3)_2$, and $Cr(NO_3)_3$, followed by a calcination at 800 ^oC for 20 h. Benzoyl peroxide acted as the oxidizer. $LiBO_2$, H_3BO_3 and $NH_4H_2PO_4$ were then mixed with the as prepared Cr-LNMO in a well designed mole ratio. After a calcination at 350 ^oC for 7 h in air, LBPO coated $LiNi_{0.45}Cr_{0.1}Mn_{1.45}O_4$ (LBPO-Cr-LNMO) was obtained. For comparison, the bare LNMO without Cr-doping was also prepared in the similar procedures.

Fig. 1a shows the X-ray diffraction patterns (XRD) of the as-prepared LNMO, Cr-LNMO and LBPO-Cr-LNMO powders. The LNMO powder has been indexed by the cubic $P4_332$ (P phase) symmetry due to the appearances of the very weak peaks located at $2\theta = 15.3^o$, 39.7^o, 45.7^o, and 57.5^o, while Cr-LNMO and LBPO-Cr-LNMO powders fit into $Fd\bar{3}m$ (F phase), in which these peaks are absent. This is in agreement with the previous reports.[20] It should be noted that in XRD patterns the P phase is very close to the F phase. Furthermore, the two phases are usually hybridized together which indicates more difficulties to differentiate them using XRD patterns.[21,22] In fact however, the two phases differ considerably with each other since the mole ratio between Mn^{3+} and Mn^{4+} is much larger in F phase than in P phase.[23,24] And the difference should be observed in cyclic voltammetry (CV) curves.

Cr^{3+} plays an important role in changing the P phase to the F phase. For the P phase spinel, characteristic impurity peaks for rock-salt $Li_xNi_{1-x}O$ phase are found in the angle regions near (222), (400) and (440) peaks which are indicated with small angled arrows in Fig. 1 (a). However, these diffractions are not observed for both Cr-LNMO and LBPO-Cr-LNMO, implying that the doping of Cr^{3+} effectively suppresses the formation of nickel oxide-like impurities which would favor the electrochemical performances.[25,26]

In the case of the LBPO, as no significant differences have been obtained in the crystal structure of the host before and after coating, we believe that the LBPO layer has formed as a separate layer on the surface of the LNMO particles and there is no evidence on the formation of a diffused layer. Since no LBPO peaks are presented in XRD, the coating layer would appear in an amorphous state, which is understandable since the layer is formed at the temperature as low as 350 ^oC.[27]

The morphology and size distribution of the three samples are compared in Fig. 1 b–d. The Cr-doping clearly influences the particle shape. LNMO (Fig. 1b) displays surfaces with less corner angle, whereas, Cr-LNMO (Fig. 1c) and LBPO-Cr-LNMO (Fig. 1d) show octahedral or pseudo-polyhedral morphology with much smoother and more complete surface facets. The particle size distribution of the three samples range from 100 nm to 1 μm which would favor the diffusion of Li^+ in the electrode.[28]

To study the LBPO-coating, the LBPO-Cr-LNMO sample has been subjected to transmission electron microscopy (TEM). The results are shown in Fig. 2. The particles exhibit polyhedral shapes with well-defined edges and corners which are clearly visible in Fig. 2a. Fig. 2b presents a continuous coating layer with a thickness of about 5 nm. The fringe patterns in Fig. 2c reveal formation of an amorphous layer on the surface of the highly crystalline Cr-LNMO spinel. The lattice distance is about 0.477 nm along the (111) directions, estimated by the FFT and the inverse FTT in the inset. To gain more insights into the crystal structure, the electron diffraction pattern of LBPO-Cr-LNMO in the $[\bar{2}33]$ zone was measured. As can be seen in Fig. 2d, the sample exhibits a typical spinel diffraction pattern which is assigned to be $Fd\bar{3}m$ symmetry, where the Li (8a), Ni (16d), Mn (16d) and O (32e) are occupying different sites.[23] According to the study of Liu et al., Cr^{3+} substitutes equal amounts of Ni^{2+} and Mn^{4+}, so we believe that Cr^{3+} occupies 16d site in the matrix.[15,29]

Fig. 3 shows Energy dispersive analysis of X-rays (EDAX) analysis on the sample. Fig. 3a shows the area of the EDAX. After a pellet was pressed at 3 MPa, the particles manifest irregular shapes with some agglomeration. The energy dispersive X-ray elemental maps of O, Mn, Ni, Cr and P were explored in this area as respectively displayed in Fig. 3b–f. The map of O illustrated in Fig. 3b sensitively depicts the outlines of the particles shown in Fig. 3a, which indicates that the as-prepared sample is homogenous. The Mn, and Ni elements also show homogeneous distribution. The map of Cr indicates that its doping is also homogeneous and effective. The map of P in Fig. 3f is an important evidence to validate the presence of the LBPO layer. The slightly dark area located at the heart of the map corresponds approximately to the largest particle in Fig. 3a, and the rest bright area corresponds to the small particles. The result indicates that LBPO distributed homogenously on the surface of the host particles. The uniform and complete coating layer was expected to stabilize the interface and electrolyte during cycling.[30] The energy dispersive spectrum (EDS), in Fig. 3g, confirms that the average chemical composition of LBPO-Cr-LNMO agrees to the designed value. The scan region of the EDS covers all of the area shown in Fig. 3a.

The Li insertion/extraction behaviours of the bare and modified samples were characterized by CV and galvanostatic charge-discharge between 3.5 V and 4.95 V, as shown in Fig. 4. All of the samples exhibit two redox areas split at 4.3 V. In the low potential area below 4.3 V, a pair of broad current bands owing to the Mn^{3+}/Mn^{4+} redox couple can be observed around 4.0 V. For the bare sample the redox peak is very weak, and for the modified samples the redox peaks are obvious, which refers to a structural difference between the bare and the modified samples. As has been discussed in XRD results in Fig. 1, the difference arises from the differentiation between $P4_332$ and $Fd\bar{3}m$ space group which belongs to the bare sample and the modified samples, respectively. Since Mn^{+3} is electrochemically more active than Mn^{4+}, the mole ratio of Mn^{3+}/Mn^{4+} should be high in F phase than in P phase. This is understandable since the oxygen loss of the samples heated above 650 ^oC can possibly reduce the valence of Mn.[31] This result is also consistent with the previous report that Cr^{3+}

doping provided a wider plateau during charging-discharging by suppressing Mn^{3+} oxidation.[26] In the high potential area above 4.3 V, the bare and the modified samples also exhibit a difference. The bare LNMO shows a single strong redox pair at 4.83/4.62 V, corresponding to the oxidation and reduction reactions of Ni^{2+}/Ni^{4+}. However, Cr-LNMO and LBPO-Cr-LNMO samples have two pairs of redox peaks located at 4.72 and 4.80 V in the oxidation process and at 4.71 and 4.63 V in the reduction process, due to the reversible reactions of the Ni^{2+}/Ni^{3+} and Ni^{3+}/Ni^{4+} couples.[20,31] The difference of the redox peaks is because the stoichiometric LNMO without any oxygen deficiency ($P4_332$) has two successive two-phase reactions ($LiNi_{0.5}Mn_{1.5}O_4$ + $Li_{0.5}Ni_{0.5}Mn_{1.5}O_4$ and $Li_{0.5}Ni_{0.5}Mn_{1.5}O_4$ + $Ni_{0.5}Mn_{1.5}O_4$) occurring at about 4.7 V, while Cr-LNMO ($Fd\bar{3}m$) experiences a solid solution reaction.[24] The latter is obviously beneficial to Li^+ transport because of the reduced number of phase boundaries that Li ions have to overcome.[24] Fig. 4b shows the initial charge and discharge profiles of the three samples at a constant current of 1 C (1 C = 146 mA h g^{-1}). The LBPO-Cr-LNMO sample presents discharge capacity of 137.1 mA h g^{-1}, a little higher than that of bare LNMO (135.2 mA h g^{-1}) and Cr-LNMO (135.6 mA h g^{-1}). It has been reported that the coating method can enhance the discharge capacity.[32–34] The reason might be that the side reactions and conductivity have a great influence on the capacity at high voltage. LBPO coating layer acts as both a protection shell and a favourable Li^+ diffusion channel, showing a much more stable surface chemistry and low charge transfer resistance. These two factors can reduce the energy consumption, resulting an elevated discharge capacity.

Fig. 5a shows the Nyquist plot of the bare and the modified samples after the first cycle at the full charged state at 4.95 V. Here, the stability of the electrolyte at high voltage is one of the crucial factors being responsible for the capacity loss, so the EIS of the full charged battery was presented. As has been described in previous work, the intercept of the plot at Z′ axis is due to the combined resistance of the electrolyte and cell components (R_e).[35] The high and intermediate frequency area appears as a contribution of two semicircles.[36] The semicircle in the high frequency is related to the resistance for Li ion migration through the surface film (R_s) and film capacitance, which indicates the appearance of a solid electrolyte interface (SEI). The semicircle in the intermediate frequency is related to charge transfer resistance (R_{ct}).[37] The quasi-straight line in the low frequency is attributed to lithium ion diffusion in the bulk materials,[38] the Warburg impedance (W). The inset shows the equivalent circuit model of the Nyquist plots.

Clearly, the values of R_{ct} increase in the order LBPO-Cr-LNMO < Cr-LNMO < LNMO. This observation suggests that the ion-conductive coating layer can effectively reduce the barrier for Li^+ transfer at intergranular interface. In addition, Cr^{3+} ion doping improves the electronic conductivity of active materials as well. The value order of R_{ct} has no change in the extended cycles as shown in Fig. S4a (50^{th} cycle) and S4b (100^{th} cycle). It should be noticed that with the extended life tests, the two semicircles presented in Fig. 5a is replaced gradually by one semicircle. There are two possibilities to understand the phenomena. One is that the two semicircles merge into a single semicircle which means the SEI still exists. And the other suggests that the SEI has actually vanished since the rate for the generation of SEI is lower than the rate for decomposition due to high potential between the electrolyte and the electrode. Our result supports the latter view since the cycle lives for the three samples are different as shown in Fig. 5b. If the SEI still remains, the cycle performances should be of little difference because of the protecting effect of the SEI layer.

Fig. 5b shows the extended cycle lives of the three samples. As measured, a reversible capacity of about 101.1 mA h g^{-1}, 74.5% capacity retention can be retained for the bare LNMO cathode over 400 cycles. The Cr-LNMO electrode delivers a discharge capacity of 115.9 mA h g^{-1}, 85.4% capacity retention with the same cycles. The cycling performances of the LBPO-Cr-LNMO sample outperform others. After 400 cycles, 125.1 mA h g^{-1}, 91.3% capacity retention is maintained. Obviously, the order of the cyclability, LBPO-Cr-LNMO > Cr-LNMO > LNMO, is in the reverse order with the values of R_{ct}. The result indicates that although the SEI is destroyed, the LBPO layer can still protect the host against the attack of the electrolyte. The bare sample manifests weak capacity retention as compared to the modified samples, which can be interpreted by the fact that the bare sample contains $Li_xNi_{1-x}O$ impurity phases which tend to react with the electrolyte and thus causes significant polarization increase and severe capacity fading.[39] Benefited with Cr-doping, the Cr-LNMO exhibits better cycle life than bare LNMO, which might be ascribed to that Cr-substitution weakens the side-reactions.[29] Undoubtedly, the LBPO coating layer is a key issue for better performances. In addition to suppressing the undesired side reactions to a greater extent through keeping the Cr-LNMO particles from direct contact with the electrolyte,[40] the LBPO coating layer enables rapid Li ion transport, which leads to faster charge transfer kinetics. The related result is shown in Table. S1−S4, where the diffusion coefficient of the LBPO-Cr-LNMO is found to be greatly enhanced compared with the other samples.

The rate performance further clarifies the function of the LBPO. As shown in Fig. 5c, the three samples were cycled at various discharge rates (1, 2, 5, 10, 20, 50 C). The constant charge rate is 1 C (1 C = 146 mA h g^{-1}). An apparent capacity fading was found in LNMO cycled at the discharge rates of 20 C and 50 C, where the discharge capacity is 90.7 mA h g^{-1} and 46.6 mA h g^{-1}, about 67.1% and 34.5% capacity retention, respectively. As has been discussed in CV results, the increased phase boundaries weaken the movement of lithium ions. In contrast, the Cr-LNMO cathode displayed an improved electrochemical performance, 105.4 and 70.9 mA h g^{-1}, 77.7% and 52.3% capacity residue respectively, at the same C rates. It can be ascribed to the increase in electrical conductivity and structural stability caused by Cr substitution for Ni and Mn.[41] There is no doubt that the coated sample exhibits much higher rate capability than the two others. LBPO-Cr-LNMO delivers a remarkable capacity of 119.3 and 81.1 mA h g^{-1}, namely, 87.0% and 59.2% capacity retention, respectively, even at high rates of 20 C and 50 C. When returned to 1 C from 50 C gradually, about 97.1 % of reversible capacity was retained for LBPO-Cr-LNMO vs. 94.2% for Cr-LNMO. This observation suggests that the coating layer which serves as an ionic conductor is favourable for Li ion transport at the electrode-electrolyte interface.[42]

Fig. 5d compares the discharge profiles of LBPO-Cr-LNMO at different C rates. It is observed that the sample shows a capacity loss from 136.9 mA h g^{-1} at 1 C to 81.1 mA h g^{-1} at 50 C, with the average discharge voltage decreasing from 4.67 V to 3.8 V, which further demonstrates its excellent rate performance. This is reasonable since a cell usually operates close to equilibrium condition at low rates, whereas the electrode overpotential and internal ohmic (IR) drop increase at high rates.[21]

In conclusion, we have proved the positive impacts of LBPO coating combined with Cr^{3+} doping on electrochemical performances of LNMO. LBPO plays an indispensable role in improving Li^+ transference and suppressing the undesired side reactions between the host and the electrolyte. The compatibility between LBPO and the host makes the material a good kind of ionic coating layer. On the other

hand, Cr^{3+} doping effectively reduces the $Li_xNi_{1-x}O$ impurity phase and lattice strain during cycling. When cycled at 1 C rate between 3.5 V and 4.95 V, about 91.3% of initial capacity can be obtained after 400 cycles for nanoscale LBPO-coated Cr-LNMO; even at 50 C rate, it delivers a reversible capacity of 81 mA h g^{-1}. The combination of $Li_{0.1}B_{0.967}PO_4$ coating and the Cr^{3+}-doping carries out a successful modification on the matrix of $LiNi_{0.5}Mn_{1.5}O_4$. We believe that the modification from the inner lattice to the outer surface should eventually lead to advanced materials that would meet the high performance requirements of lithium ion batteries.

Acknowledgements

This work was supported by the National Science Foundation of China (no. 51273027).

Notes and references

* *Jiangsu Key Laboratory of Advanced Catalytic Materials and Technology, Changzhou University, Changzhou 213164, China. E-mail: jinhongshi0001@163.com*

† Electronic Supplementary Information (ESI) available: See DOI: 10.1039/b000000x/

1 G. N. Zhu, Y. G. Wang and Y. Y. Xia, *Energy Environ. Sci.*, 2012, 5, 6652–6667.

2 H. S. Zhou, *Energy Environ. Sci.*, 2013, 6, 2256–2256.

3 J. Hassoun, S. Panero, P. Reale and B. Scrosati, *Adv. Mater.*, 2009, 21, 4807–4810.

4 J. R. Szczech and S. Jin, *Energy Environ. Sci.*, 2011, 4, 56–72.

5 K. R. Chemelewski and A. Manthiram, *J. Phys. Chem. C*, 2013, 117, 12465−12471.

6 Y. Y. Huang, X. L. Zeng, C. Zhou, P. Wu and D. G. Tong, *J. Mater. Sci.*, 2013, 48, 625–635.

7 J. Liu and A. Manthiram, *Chem. Mater.*, 2009, 21, 1695−1707.

8 S. Mukerjee, X. Q. Yang, X. Sun, S. J. Lee, J. McBreen and Y. Ein-Eli, *Electrochim. Acta*, 2004, 49, 3373–3382.

9 T. A. Arunkumar and A. Manthiram, *Electrochem. Solid-State Lett.*, 2005, 8, A403−A405.

10 Y. K. Sun, K. J. Hong, J. Prakash and K. Amine, *Electrochem. Commun.*, 2002, 4, 344–348.

11 Y. K. Sun, C. S. Yoon and I. H. Oh, *Electrochim. Acta*, 2003, 48, 503–506.

12 R. Alcantara, M. Jaraba, P. Lavela and J. L. Tirado, *J. Electroanal. Chem.*, 2004, 566, 187–192.

13 T. Noguchi, I. Yamazaki, T. Numata and M. Shirakata, *J. Power Sources*, 2007, 174, 359–365.

14 Y. K. Sun, S. T. Myung, B. C. Park, J. Prakash, I. Belharouak and K. Amine, *Nat. Mater.*, 2009, 8, 320–324.

15 D. Liu, J. Hamel-Paquet, J. Trottier, F. Barray, V. Gariepy, P. Hovington, A. Guerfi, A. Mauger, C. M. Julien, J. B. Goodenough and K. Zaghib, *J. Power Sources*, 2012, 217, 400–406.

16 J. C. Li, L. Baggetto, S. K. Martha, G. M. Veith, J. Nanda, C. D. Liang and N. J. Dudney, *Adv. Energy Mater.*, 2013, 3, 1275-1278.

17 J. Chong, S. D. Xun, X. Y. Song, G. Liu and V. S. Battaglia, *Nano Energy*, 2013, 2, 282–293.

18 J. H. Cho, J. H. Park, M. H. Lee, H. K. Song and S. Y. Lee, *Energy Environ. Sci.*, 2012, 5, 7124–7131.

19 M. J. G. Jak, E. M. Kelder, J. Schoonman, N. M. Van Der Pers and A. Weisenburger, *J. Electroceram*, 1998, 2, 127–134.

20 G. B. Zhong, Y. Y. Wang, Y. Q. Yu and C. H. Chen, *J. Power Sources*, 2012, 205, 385–393.

21 X. L. Zhang, F. Y. Cheng, K. Zhang, Y. L. Liang, S. Q. Yang, J. Liang and J. Chen, *RSC Adv.*, 2012, 2, 5669–5675.

22 J. Cabana, M. Casas-Cabanas, F. O. Omenya, N. A. Chernova, D. L. Zeng, M. S. Whittingham and C. P. Grey. *Chem. Mater.*, 2012, 24, 2952–2964.

23 J. H. Kim, S. T. Myung, C. S. Yoon, S. G. Kang and Y. K. Sun, *Chem. Mater.*, 2004, 16, 906–914.

24 J. M. Zheng, J. Xiao, X. Q. Yu, L. Kovarik, M. Gu, F. Omenya, X. L. Chen, X. Q. Yang, J. Liu, G. L. Graff, M. S. Whittingham and J. G. Zhang, *Phys. Chem. Chem. Phys.*, 2012, 14, 13515–13521.

25 S. H. Oh, K. Y. Chung, S. H. Jeon, C. S. Kim, W. I. Cho and B. W. Cho, *J. Alloys Compd.*, 2009, 469, 244–250.

26 S. B. Park, W. S. Eom, W. I. Cho and H. Jang, *J. Power Sources*, 2006, 159, 679–684.

27 M. J. G. Jak, E. M. Kelder and S. J. Everstein, J. Schoonman, *J. Power Sources*, 1999, 81–82, 808–812.

28 T. F. Yi, C. Y. Li, Y. R. Zhu, J. Shu and R. S. Zhu, *J. Solid State Electrochem.*, 2009, 13, 913–919.

29 D. Liu, Y. Lu and J. B. Goodenough, *J. Electrochem. Soc.*, 2010, 157, A1269–A1273.

30 W. Liu, M. Wang, X. L. Gao, W. D. Zhang, J. T. Chen, H. H. Zhou and X. X. Zhang, *J. Alloys Compd.*, 2012, 543, 181–188.

31 Z. X. Chen, S. Qiu, Y. L. Cao, X. P. Ai, K. Xie, X. B. Hong and H. X. Yang, *J. Mater. Chem.*, 2012, 22, 17768–17772.

32 H. B. Kim, B. C. Park, S. T. Myung, K. Amine, J. Prakash and Y. K. Sun, *J. Power Sources*, 2008, 179, 347–350.

33 B. C. Park, H. B. Kim, S. T. Myung, K. Amine, I. Belharouak, S. M. Lee and Y. K. Sun, *J. Power Sources*, 2008, 178, 826–831.

34 D. J. Lee, K. S. Lee, S. T. Myung, H. Yashiro and Y. K. Sun, *J. Power Sources*, 2011, 196, 1353–1357.

35 K. M. Shaju, G. V. Subba Rao and B. V. R. Chowdari, *J. Electrochem. Soc.*, 2004, 151, A1324–A1332.

36 J. L. Li, C. B. Cao, X. Y. Xu, Y. Q. Zhu and R. M. Yao, *J. Mater. Chem. A*, 2013, 1, 11848–11852.

37 Y. Y. Cho, P. G. Oh and J. P. Cho, *Nano Lett.*, 2013, 13, 1145–1152.

38 J. Liu and A. Manthiram, *J. Electrochem. Soc.*, 2009, 156, A66–A72.

39 R. Santhanam and B. Rambabu, *J. Power Sources*, 2010, 195, 5442–5451.

40 D. Liu, J. Trottier, P. Charest, J. Frechette, A. Guerfi, A. Mauger, C. M. Julien and K. Zaghib, *J. Power Sources*, 2012, 204, 127–132.

41 M. W. Jang, H. G. Jung, B. Scrosati and Y. K. Sun, *J. Power Sources*, 2012, 220, 354–359.

42 J. Lu, Q. Peng, W. Y. Wang, G. Y. Nan, L. H. Li and Y. D. Li, *J. Am. Chem. Soc.*, 2013, 135, 1649–1652.

Figure Captions:

Scheme 1 Schematic illustration of the preparation of $Li_{0.1}B_{0.967}PO_4$-coated $LiNi_{0.45}Cr_{0.1}Mn_{1.45}O_4$.

Fig. 1 (a) XRD patterns of the as-prepared samples and FESEM images of (b) LNMO, (c) Cr-LNMO and (d) LBPO-Cr-LNMO.

Fig. 2 (a, b) TEM, (c) HRTEM and (d) SAED pattern of LBPO-Cr-LNMO. The insets of (c) show the fast Fourier transformation (FFT) of the HRTEM image and the Inverse FFT, respectively.

Fig. 3 (a) FESEM image of LBPO-Cr-LNMO and elemental maps for (b) O, (c) Mn, (d) Ni, (e) Cr, (f) P and (g) EDX of LBPO-Cr-LNMO. The inset table in (g) denotes the average chemical composition of LBPO-Cr-LNMO.

Fig. 4 (a) CV curves at a scan rate of 0.1 mV s^{-1} and (b) initial charge-discharge profiles of LNMO, Cr-LNMO and LBPO-Cr-LNMO at a current of 146 mA h g^{-1}.

Fig. 5 (a) Nyquist plots of LNMO, Cr-LNMO and LBPO-Cr-LNMO with a frequency range from 65 kHz to 0.1 Hz at the 1^{st} cycle in the charged state of 4.95V. (b) Cycling performance at 1 C (146 mA h g^{-1}). (c) Cycling performance at various rates (charge at 1 C) and (d) Discharge profiles of LBPO-Cr-LNMO at various rates between 3.5 and 4.95 V.

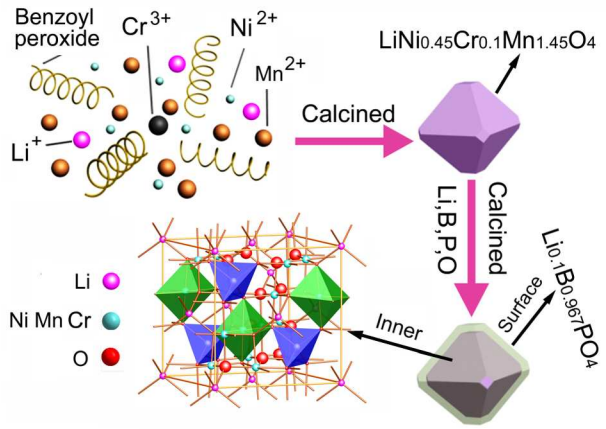

Scheme 1

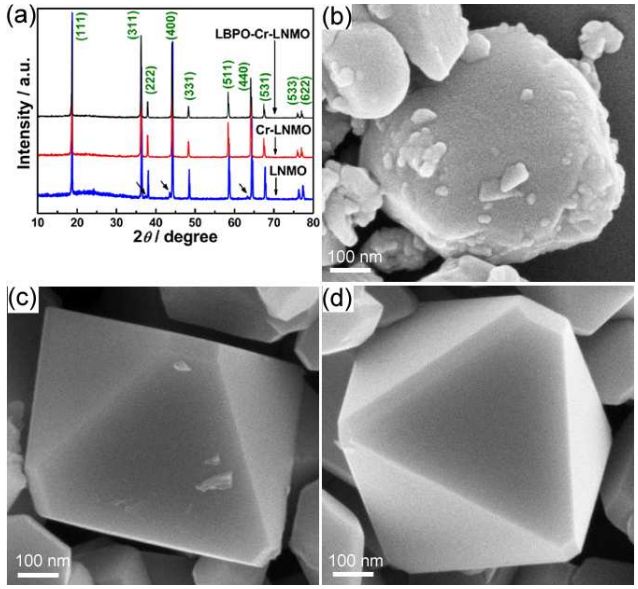

Fig. 1

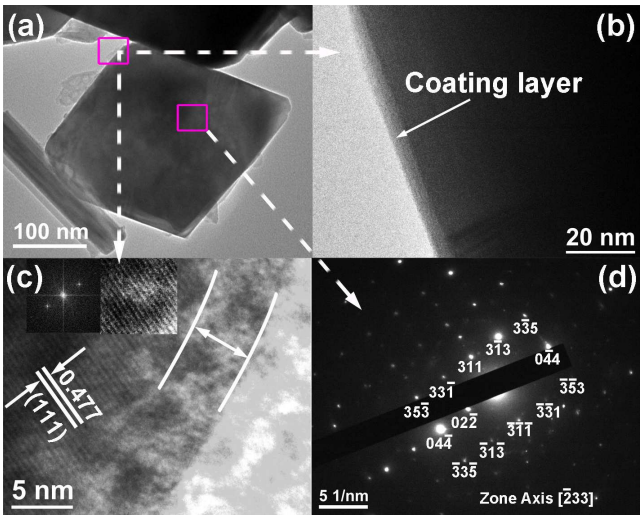
(a)
(b)
Coating layer
100 nm
20 nm
(c)
(d)
0.477
(111)
5 nm
5 1/nm
Zone Axis [2̄33]

Fig. 2

5

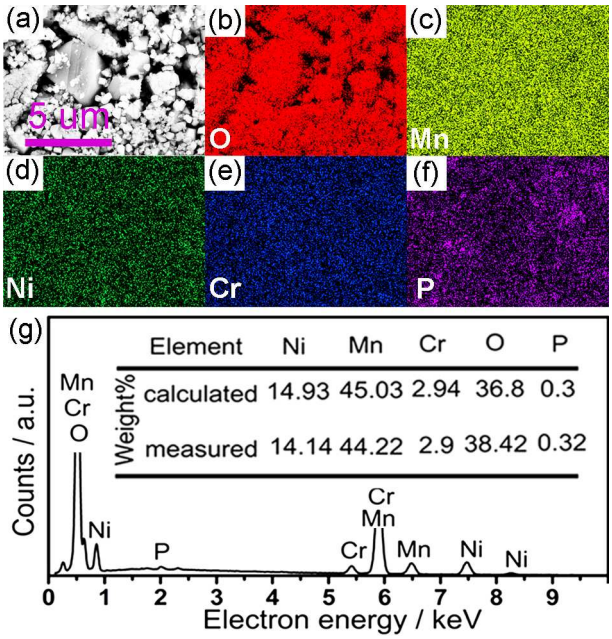
(a)
(b)
(c)
5 um
O
Mn
(d)
(e)
(f)
Ni
Cr
P
(g)
Element Ni Mn Cr O P
Weight% calculated 14.93 45.03 2.94 36.8 0.3
measured 14.14 44.22 2.9 38.42 0.32
Mn
Cr
O
Ni
P
Cr
Mn
Cr
Mn
Ni
Ni
Counts / a.u.
0 1 2 3 4 5 6 7 8 9
Electron energy / keV

Fig. 3

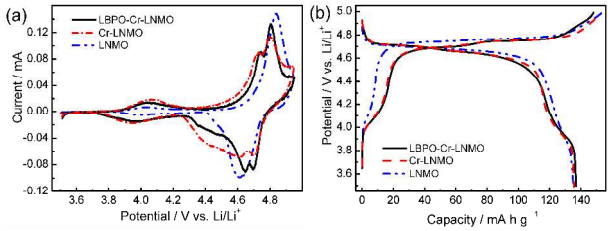
(a)
LBPO-Cr-LNMO
Cr-LNMO
LNMO
Current / mA
Potential / V vs. Li/Li+
(b)
Potential / V vs. Li/Li+
Capacity / mA h g-1
LBPO-Cr-LNMO
Cr-LNMO
LNMO

Fig. 4

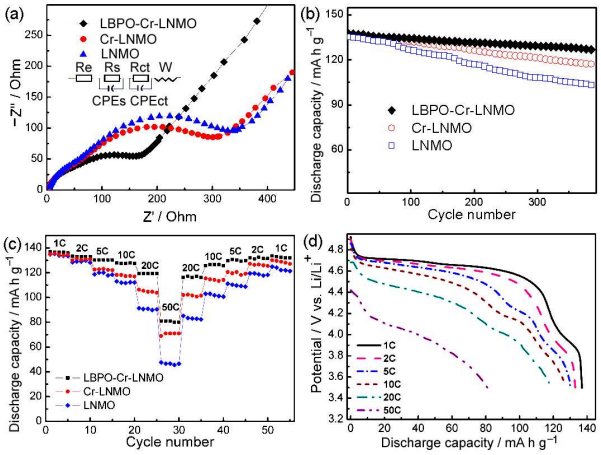
(a)
LBPO-Cr-LNMO
Cr-LNMO
LNMO
Re Rs Rct W
CPEs CPEct
-Z'' / Ohm
Z' / Ohm
(b)
Discharge capacity / mA h g-1
Cycle number
LBPO-Cr-LNMO
Cr-LNMO
LNMO
(c)
1C 2C 5C 10C 20C 50C
Discharge capacity / mA h g-1
Cycle number
LBPO-Cr-LNMO
Cr-LNMO
LNMO
(d)
Potential / V vs. Li/Li+
Discharge capacity / mA h g-1
1C
2C
5C
10C
20C
50C

Fig. 5

Colour graphic:

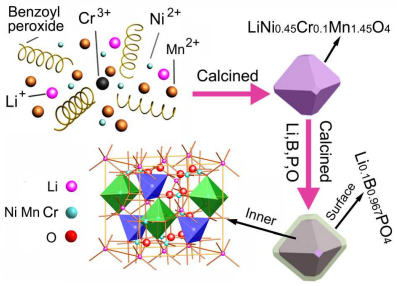

Highlighting:

The $Li_{0.1}B_{0.967}PO_4$ Li^+-conductive coater improves the cyclability and rate performance of Cr^{3+} doped $LiNi_{0.5}Mn_{1.5}O_4$ high potential cathode.